



Prediction of field-dependent rheological properties of magnetorheological grease using extreme learning machine method

Irfan Bahiuddin^{1,2} , Nurul AA Wahab¹, Mohd I Shapiai¹, Saiful A Mazlan¹, Norzilawati Mohamad¹ , Fitriani Imaduddin³ and Ubaidillah³

Journal of Intelligent Material Systems and Structures

2019, Vol. 30(11) 1727–1742

© The Author(s) 2019

Article reuse guidelines:

sagepub.com/journals-permissions

DOI: 10.1177/1045389X19844007

journals.sagepub.com/home/jim



Abstract

Magnetorheological grease is seen as a promising material for replacing the magnetorheological fluid owing to its higher stability and the lesser production of leakage. As such, it is important that the rheological properties of the magnetorheological grease as a function of a composition are conducted in the modeling studies of a magnetorheological grease model so that its optimum properties, as well as the time and cost reduction in the development process, can be achieved. Therefore, this article had proposed a machine learning method-based simulation model via the extreme learning machine and backpropagation artificial neural network methods for characterizing and predicting the relationship of the magnetorheological grease rheological properties with shear rate, magnetic field, and its compositional elements. The results were then evaluated and compared with a constitutive equation known as the state transition equation. Apart from the shear stress results, where it had demonstrated the extreme learning machine models as having a better performance than the other methods with R^2 more than 0.950 in the training and testing data, the predicted rheological variables such as shear stress, yield stress, and apparent viscosity were also proven to have an agreeable accuracy with the experimental data.

Keywords

Magnetorheological grease, neural networks, machine learning, composition, extreme learning machine, rheology

1. Introduction

Magnetorheological (MR) grease belongs to a smart materials class, where the millisecond changes on their controllable and reversible rheological properties can be modified by using the magnetic field as an external stimulus, where it causes the micron size magnetic particle to build a chain-like structure within the grease as the carrier fluid (Choi et al., 2014; Xu et al., 2018). Apart from overcoming the drawbacks of the MR fluid's weak stability and leakage issues (Shilan et al., 2016), the use of MR grease was also developed to abate the sedimentation issue of the hydrocarbon oil in the MR fluids. The MR grease had prevented the falling of the carbonyl iron particles (CIPs) despite the density mismatch between the particle and the carrier fluid. To improve the materials performance and understand the behavior, some works have investigated the influencing factors of the material composition, such as the addition of weight percentage on the CIPs (Mohamad et al., 2016), the utilization of the medium oil as an

additive (Kim et al., 2012), and the effect of various particle shapes (Mohamad et al., 2018; Wei et al., 2012). From the obtained results, the mechanism and correlations between the compositions and the MR grease were found to have exhibited a complex pattern or behavior, particularly on the composition effect

¹Malaysia-Japan International Institute of Technology, Universiti Teknologi Malaysia, Kuala Lumpur, Malaysia

²Department of Mechanical Engineering, Vocational School, Universitas Gadjah Mada, Yogyakarta, Indonesia

³Mechanical Engineering Department, Faculty of Engineering, Universitas Sebelas Maret, Surakarta, Indonesia

Corresponding authors:

Mohd I Shapiai, Malaysia-Japan International Institute of Technology, Universiti Teknologi Malaysia, 54100 Kuala Lumpur, Malaysia.
Email: md_ibrahim83@utm.my

Saiful A Mazlan, Malaysia-Japan International Institute of Technology, Universiti Teknologi Malaysia, 54100 Kuala Lumpur, Malaysia.
Email: amri.kl@utm.my

toward the shear and yield stress as well as the apparent viscosity. Since material development is not only time-consuming but also requires an enormous amount of workforce and cost material, the introduction of a constitutive model can, therefore, be used as a tool in expediting the development process.

For this reason, the model that is to be developed has to be able to significantly capture the behavioral changes of the MR grease materials such as the volume fraction (Jung et al., 2016; Varela-Jiménez et al., 2015) as well as the operating variables like those of shear rates and magnetic fields (Mohamad et al., 2018). In other words, the model formulation has to be developed based on the intended applications such as those of rheological characterizations (Cvek et al., 2016; Ghaffari et al., 2015) and control designs (Chang and Zhou, 2002). Although the same Bingham plastic and Herschel–Bulkley models had been utilized from those in the MR fluid (Ghaffari et al., 2015), these models were nevertheless modified in the study of the MR grease properties. Generally, the MR grease can be classified as a thixotropic material or semi-solid MR material and with an initial yield stress at off-state condition (without applied magnetic field) (Mohamad et al., 2016). It has the tendency of exhibiting a non-Newtonian fluid trait as opposed to the Newtonian characteristic shown by the MR fluid at off-state condition. For example, although the previous studies had tried to accommodate for the composition parameters of the MR materials (Varela-Jiménez et al., 2015), the model has difficulty in estimating other variables for rheometer characterization such as viscosity, shear stress, and shear rate, because the model directly predicts the yield stress. For this reason, one of the possible ways of solving this issue can be through the introduction of a flexible model with a capability for duplicating the highly non-linear material behavior.

Machine learning is not only proven to be a powerful tool for learning the material properties of the experimental data as well as to predict the unlearned data (Mueller et al., 2016; Zhang and Friedrich, 2003), but is also widely used in the study of the MR materials (Imaduddin et al., 2017; Wang and Liao, 2005). The methods can be selected from the existing studies, such as backpropagation artificial neural network (BP-ANN) (Shahriar and Nehdi, 2011; Vani et al., 2015), support vector regression (SVR) (Liu and Chen, 2013; Liu et al., 2014), extreme learning machine (ELM) (Jin et al., 2017; Zheng et al., 2017), and deep learning (DL) (Liu et al., 2017, 2018). ELM (Jin et al., 2017; Zheng et al., 2017) is known for its shorter training time as well as its better accuracy (Li et al., 2016; Zheng et al., 2018) and generalization levels than the conventional SVR and BP-ANN methods (Huang et al., 2011, 2015). On the other hand, DL is known for its capability to predict a complex behavior of a system with higher training time than ELM because the DL algorithm tries

to adjust all layers and usually involves multilayer hidden nodes neural networks (Tang et al., 2015, 2016). With those advantages, ELM has been applied in MR liquids (MR fluid and grease) utilizing ELM to predict the shear stress as a function of magnetic, shear rate (Bahiuddin et al., 2017, 2018a, 2019), and temperature (Bahiuddin et al., 2018b).

However, the study on the model formulation MR grease as a function of composition, especially CIPs concentration, using machine learning technique has not been reported yet as the authors' best knowledge. In the machine learning application of other materials that predict viscosity (Zheng et al., 2017) and shear stress (Khozani et al., 2017), the models have not covered magnetic field as one of the inputs. Furthermore, some materials have different properties when compared to MR liquids, such as viscoelastic and solid materials (Bobbili et al., 2014; Jin et al., 2017). Therefore, the technical novelty of this study had been the proposed use of an ELM and BP-ANN-based constitutive model in the prediction of the MR grease rheological properties as a result of the composition effects. The normalization of the ELM inputs through the use of a logarithm equation as opposed to the linear normalization method also has been investigated. The platform also accommodated the prediction of the shear stress, shear yield stress, and apparent viscosity based on rotational rheometer test. The discussion will begin by describing the primary indicator of grease performance, which is then followed by the modeling concept, material properties, material preparation, and finally, the setting up of the model.

2. The existing models and performance indicator of MR grease

2.1. The existing models of MR grease

Since both the MR grease and fluid possess many similarities with regard to the characterization methods and material behavior, the prediction on the MR grease's rheological behavior can, therefore, be carried out by adopting the rheological models used in the MR fluid models. The most common model that is used for the MR fluid had been the Bingham plastic (Ghaffari et al., 2015), which is expressed in equation (1)

$$\tau = \tau_y + \eta \dot{\gamma} \quad \text{for } \tau > \tau_y \quad (1)$$

where τ is the shear stress, τ_y is the yield stress, η is the plastic viscosity, and $\dot{\gamma}$ is the shear rate. However, the Bingham plastic is often regarded as being a simple model, where its accuracy level is only restricted to either the low or high shear rate ranges (Ghaffari et al., 2015). For this reason, several rheological models such as the Herschel–Bulkley (Farjoud et al., 2008), Casson (Papanastasiou and Boudouvis, 1997) and the

Robertson stiff (Cvek et al., 2016) had attempted to overcome the shortcomings by adding one more parameters in their respective equations. While the Casson model (Papanastasiou and Boudouvis, 1997) had been similar to that of the Herschel–Bulkley, the Robertson-stiff model (Cvek et al., 2016) however, was found to have produced a better accuracy level than the Herschel–Bulkley model. There were also other researchers who had proposed using different models by separating the equation according to the critical shear rate value ($\dot{\gamma}_c$) and dividing the shear rate into two different regions. For example, biplastic Bingham (Dimock et al., 2000, 2002) has used Bingham plastic equation for both lower and higher than critical shear rates. Another similar model with biplastic Bingham is biviscous model (Choi et al., 2005) by assuming the fluid behaves like a Newtonian fluid at a low shear rate and a non-Newtonian fluid at a high shear rate. Papanastasiou (1987) also tried to form a model by defining a single equation that consists of equations for low and high shear rate region.

It is noted that all models have a similarity with Bingham plastic model, which are shear stress as the output and shear rate as the input. The two variables are the essential variables in a flow curve as the measurement results from the rheometer test. The other model to predict MR grease/gel behavior as a function of the additional variables other than shear rate is a model that includes temperature to predict the yield stress (Sahin et al., 2009). If the model is required to include a composition as one of the inputs, another existing or a new model needs to be adopted.

The models that are capable to accommodate weight percentage of magnetic particles as an input can be considered rare (Jung et al., 2016; Sahin et al., 2009). For example, Varela-Jiménez et al. (2015) developed an MR fluid model to predict yield stress as a function of magnetic field and volume fraction called state transition equation (STE). This model was derived based on the concept of state transition when the MR fluid changes from liquid to semi-solid state. The mathematical expression of the model is shown at equation (2)

$$\tau_y = \left[1 + \left(\frac{B}{\alpha\varphi^2 + \beta_V\varphi + \lambda} \right)^{-B_{MRF}} \right]^{-1} \left[\frac{4}{5^{\frac{3}{2}}} \xi(3) \varphi \mu_0 M_s^2 \right] \quad (2)$$

where B is the magnetic field; B_{MRF} is a constant fitted based on the experimental data of the volume fraction as a function of magnetic field; α , β_V , and λ are the polynomial constant representing the magnetic field characteristics when 50% of the state transition occurs; φ is the volume fraction; μ_0 is the permeability of vacuum; M_s is the saturation magnetic field of the material used as particles; and $\xi(3)$ is a constant determined by Ginder et al. (1996).

Despite the various developed MR fluid models, the Bingham plastic (equation (1)) and the temperature-

dependent models were the only models used in the characterization and modeling of the MR grease (Mohamad et al., 2016; Sahin et al., 2009), where the obtained plastic viscosities and yield stress of the MR grease samples could be used in the justification of the material behavior. On the other hand, a pioneer model that accommodates the composition factor such as the volume fraction can also be adopted from equation (2) as a way of comprehending the MR grease behavior. However, this model not only requires detailed material information in the estimation of its supplementary constants (Jung et al., 2016; Varela-Jiménez et al., 2015) but also requires the involvement of multiple fitting processes. It is also important to note that although a possible new equation to predict the shear stress as a function of shear rate can be derived by combining the model with the Bingham plastic as suggested by Varela-Jiménez et al. (2015), the combined model would still inherit the existing disadvantages of the Bingham plastic model. Furthermore, since the model had been developed based on the MR fluid's quasi-liquid to quasi-solid state and with on-state magnetic fields condition, the sigmoidal behavior that was observed in the MR fluid transition may not be suitable for the study of MR grease with semi-solid-state properties at an off-state condition.

2.2. MR grease performance indicator

The rheological properties of MR grease and its correlation with magnetic fields are usually carried out using rotational and oscillation test (Mohamad et al., 2016). From the rotational test, the primary obtained data in a flow curve form consist of shear stress as a function of shear rate. From the data, the derived variables can be gathered, such as dynamic yield stress, apparent yield stress, apparent viscosity, plastic viscosity, and so on. Meanwhile, from oscillation test, storage modulus and loss modulus as a function of shear strain, frequency, and magnetic fields can be obtained. This article focuses on modeling based on the data from the rotational test method.

One of the main results of the characterization using rotational test is shear stress as a function of shear rate. From the shear rate, the dynamic yield stress can be obtained. Dynamic yield stress is a critical value of the applied stress to make the material to flow and continuously break the chain-like structure (De Vicente et al., 2011). In a mathematical equation, the relation can be described as in equation (3)

$$\tau = f(\tau_y, \eta, \dot{\gamma}), \quad \dot{\gamma} = 0 \quad \text{for } |\tau| < \tau_y \quad (3)$$

where τ is the shear stress, τ_y is the dynamic yield stress, $\dot{\gamma}$ is the shear rate, and η is the plastic viscosity (Marinică et al., 2016). The function ($f(\tau_y, \eta, \dot{\gamma})$) can be Bingham plastic (Ashtiani et al., 2015; Mohamad et al., 2016), Herschel–Bulkley (Marinică et al., 2016), or others (Ghaffari et al., 2015). In addition, yield stress can

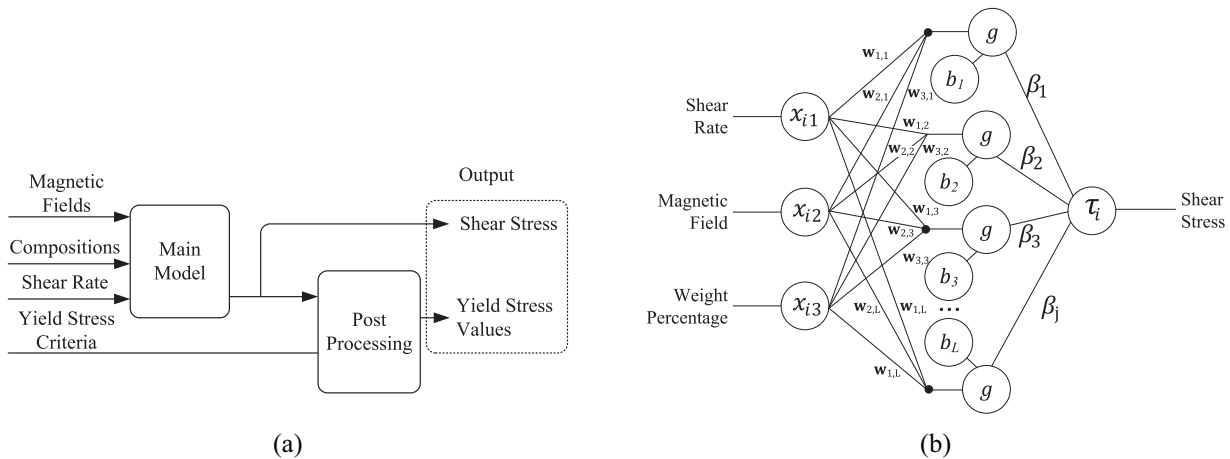


Figure 1. The proposed modeling configuration: (a) the overall system and (b) the main model.

also be determined using Bingham plastic model on a selected shear rate ranges (Sherman et al., 2015; Shilan et al., 2016). In MR damper applications, yield stress represents the damping force of an MR damper (Gurubasavaraju et al., 2017; Xu et al., 2015), while in MR brake and clutch, yield stress represents the produced torque (Bucchi et al., 2015; Karakoc et al., 2008). The higher the yield stress, the higher the device performance. The correlation between yield stress and magnetic field is also proportional within a specific magnetic field range.

Another variable to measure MR grease performance is the MR effect (Mohamad et al., 2018; Yunus et al., 2016). The MR effect is calculated based on the storage modulus. From the indicator of MR effect, the significance of magnetic fields to the material properties to store mechanical energy can be easily observed with a percentage unit. However, the MR effect can only be obtained using the oscillated test to determine the viscoelastic properties of the material. Thus, a similar method to obtain the magnetic effect on the yield stress of MR grease can be derived based on the rotational test results. Yield stress range is the possible parameter to represent the MR effect using the expression in equation (4)

$$E_{\tau_{y,B}} = \tau_{y,B} - \tau_{y,0} \quad (4)$$

where $E_{\tau_{y,B}}$ is a yield stress range to represent the magnetic field effect B toward yield stress, $\tau_{y,0}$ is the yield stress at the off-state condition, and $\tau_{y,B}$ is the yield stress at a magnetic field of B . If $\tau_{y,0}$ is significantly smaller than $\tau_{y,B}$, $\tau_{y,0}$ can be neglected leaving $\tau_{y,B}$ only to measure the performance of an MR grease.

3. The modeling platform

The MR grease performance can be measured by its primary measurement variable of shear stress in a typical rotational test (Mohamad et al., 2018; Shilan et al., 2016) as well as the derived parameters of yield stress,

plastic viscosity, and apparent viscosity from the obtained primary measurement variables. The modeling objective is to obtain the correlation between the compositions and the MR grease performance. Hence, the system can be formulated either as a simple equation that describes the performance indicator as a function of compositions, but with a compromise on the shear rate and shear stress information, or through the use of two models in the prediction of two indicators or output. Therefore, the best way of simultaneously predicting the primary variables and derived parameters as a function of compositions would be to use the proposed framework as shown in Figure 1(a).

As such, the proposed framework had been divided into two parts, namely the shear stress model for predicting the shear rate from the primary variables and the post-processing construct for the derived parameters. In other words, this model is treated as a constitutive equation with the additional magnetic field and composition inputs, where the rotational test of the model as shown in Figure 1(b) had consisted of at least three inputs (shear rate, magnetic field, and solid weight percentage) and with one output variable (shear stress).

In the second part of the model, the post-processing construct as shown in Figure 1(a) was used to calculate the derived parameters such as the yield stress and apparent viscosity. Under this construct, the yield stress was calculated by fitting the Bingham plastic model into the estimated shear stress according to a “yield stress criteria,” which will be further elaborated under section 3.2.

This model is not only easily scalable but also can be extended to the other inputs. The configuration had also offered the advantage for the material scientist to observe and duplicate the effect of the shear rate to the shear stress and in the prediction of the possible consequences exhibited by the MR grease.

3.1. Shear stress model

A neural network was structured with $\log_{10}(\dot{\gamma}_i)$, magnetic field (B_i), and weight percentage of CIPs ($w_{t,i}$) as the model inputs and shear stress ($\tau_{p,i}$) as the output. The general function can be expressed as in equation (5)

$$\tau_{p,i} = f(B_i, \dot{\gamma}_i, w_{t,i}) \tag{5}$$

Although other alternative inputs can be selected, such as temperature (T), strain rate ($\dot{\gamma}_i$), and frequency (f), B_i , $\dot{\gamma}_i$, and $w_{t,i}$ were selected with their own specific reason. $\dot{\gamma}_i$ is preferable because this research focuses to replicate the flow curve characteristic of an MR grease. B_i is selected because the mechanical behavior of MR materials is mainly affected by magnetic fields. For composition, the inputs can be volume fraction of the CIPs ($v_{f,s}$) or $w_{t,i}$. The both inputs are assumed to be interchangeable. The output can be shear stress ($\tau_{p,i}$) or yield stress ($\tau_{y,i}$) or apparent viscosity ($\eta_{a,i}$). However, the direct prediction of $\tau_{y,i}$ means the loss information of shear stress and apparent viscosity. Hence, $\tau_{p,i}$ was selected as primary output, while $\tau_{y,i}$ and $\eta_{a,i}$ were predicted as derived variables

ELM and BP-ANN methods were selected in order to obtain the shear stress model. Both models have similar basic neural networks called single-hidden layers feedforward neural network (SLFN) containing three layers, which are input, hidden node, and output layers. The SLFN parameters are weighting inputs (\mathbf{w}_j) in input layer, biases (b_j), and activation functions $G_j(\cdot)$ in the hidden node layer, and weighting outputs (β_j) in the output layer. The full form of SLFNs can be observed in Figure 1(b) with the mathematical relationship as expressed in equation (6)

$$\begin{aligned} \tau_{p,i}(B_i, \dot{\gamma}_i, w_{t,i}) &= \sum_{j=1}^L G_j(\mathbf{w}_j, b_j, B_i, \dot{\gamma}_i, w_{t,i})\beta_j \\ &= \sum_{j=1}^L h_{j,i}(B_i, \dot{\gamma}_i, w_{t,i})\beta_j \end{aligned} \tag{6}$$

where i is the variable at i th sample, L is the hidden nodes number, and j is the parameter or variable at the j th hidden node.

The logarithm normalization is needed to be carried out for the inputs of the training data. Therefore, the data can be scaled between 0 and 1. The normalization method for the shear rate and magnetic fields are expressed as follows

$$x_{1,i} = \frac{\log(\dot{\gamma}_{exp,i}) - \log(\dot{\gamma}_{min})}{\log(\dot{\gamma}_{max}) - \log(\dot{\gamma}_{min})} \tag{7}$$

$$x_{2,i} = \frac{B_{exp,i} - B_{min}}{B_{max} - B_{min}} \tag{8}$$

$$x_{3,i} = \frac{w_{t,exp,i} - w_{t,min}}{w_{t,max} - w_{t,min}} \tag{9}$$

where $x_{1,i}$, $x_{2,i}$, and $x_{3,i}$ are the first, second, and third input of the SLFNs, respectively. exp , min , and max are the experimental data, the minimum value of the measured variables, and the maximum value of the measured variables, respectively.

The BP-ANN training was carried out using neural networks toolbox (*nntoolbox*) in MATLAB. Lavenberg Marquardt (LM) is selected as the training algorithm because in another similar case the algorithm has shown its superiority compared to other algorithms provided by MATLAB (Rabbani et al., 2017). The activation function is sigmoid. Meanwhile, the ELM algorithm has some steps (Huang et al., 2011). The first step is randomly assigning w_j and β_j using a random continuous function, such as Gaussian distribution. The second step is calculating the value of hidden node output at j th hidden node number and i th sample ($h_{j,i}(B, \dot{\gamma}, w_p)$) for all hidden nodes or determining the hidden node output matrix (\mathbf{H}) as expressed in equation (10)

$$\mathbf{H} = \begin{bmatrix} g(\mathbf{w}_1, b_1, B_1, \dot{\gamma}_1, w_{p,1}) & \dots & g(\mathbf{w}_L, b_L, B_1, \dot{\gamma}_1, w_{p,1}) \\ \vdots & \dots & \vdots \\ g(\mathbf{w}_1, b_1, B_N, \dot{\gamma}_N, w_{p,N}) & \dots & g(\mathbf{w}_L, b_L, B_N, \dot{\gamma}_N, w_{p,N}) \end{bmatrix}_{N \times L} \tag{10}$$

where N is a number of samples. The last step is determining the output weight matrix (β) that is defined by equation (11)

$$\beta = \mathbf{H}^\dagger \mathbf{T}; T = \begin{bmatrix} T_1 \\ \dots \\ T_N \end{bmatrix}, \beta = \begin{bmatrix} \beta_1 \\ \dots \\ \beta_L \end{bmatrix} \tag{11}$$

where \mathbf{T} is the measured shear stress as the target for the training process, and \mathbf{H}^\dagger is Moore–Penrose generalized inverse of matrix \mathbf{H} (calculated using singular value decomposition (SVD) method) (Huang et al., 2012).

The activation function or $G(\cdot)$ can be selected from one of the existing equations, such as hard limit, sine, sigmoid, and radian basis (Bahiuddin et al., 2017; Tang et al., 2015). The hard limit, sigmoid, and sine or sinusoid function are expressed as in equations (12) to (14), respectively

$$g_j(w_j, b_j, x) = \begin{cases} 1, & \text{if } w_j \cdot x + b_j \geq 0 \\ 0, & \text{if } w_j \cdot x + b_j < 0 \end{cases} \tag{12}$$

$$g_j(w_j, b_j, x) = \frac{1}{1 + \exp(-(w_j \cdot x + b_j))} \tag{13}$$

$$g_j(w_j, b_j, x) = \sin(w_j \cdot x + b_j) \tag{14}$$

where w_j and b_j are the j th hidden node weight input and bias. x consists of the defined inputs, which are $\log_{10}(\dot{\gamma}_i)$, magnetic field (B_i), and weight percentage of CIPs ($w_{t,i}$).

3.2. Derived parameter estimation

Yield stress and apparent viscosity can be considered as derived parameters. Yield stress was calculated using Bingham plastic equation, as expressed in equation (1). By fitting the equation to the designated experimental data of a flow curve data set, the yield stress can be estimated. For example, Figure 2 shows a set of flow curve data (solid line) of shear stress as a function of shear rate. If the designated experimental data for Bingham plastic fitting is the data between $\dot{\gamma}_1$ and $\dot{\gamma}_2$, yield stress (τ_y) can be obtained when a Bingham plastic equation (dash red line) is fitted to the data. The mentioned “yield stress criteria” is the shear rate range determined by the user that will be utilized as a reference to predict yield stress (Leong et al., 2016; Shilan et al., 2016). Meanwhile, the apparent viscosity (η) is calculated using equation (15)

$$\eta = \frac{\tau}{\dot{\gamma}} \quad (15)$$

4. Experimental and simulation setup

4.1. Material preparation

The typical composition of MR grease consists of the magnetic particle and suspension medium. The CIPs were obtained from BASF Germany, type of OM. The particles have specifications with an average size of 5 μm , density of 7.874 g cm^{-3} and spherical shape form. The suspension medium is commercial grease with NLGI 3 code NPC Highrex HD-3 produced by Nippon Koyu Ltd, Japan, with density about 0.92 g cm^{-3} . The mixing process was divided into two stages. The first process is the plain grease preparation by stirring the grease for 5 min. In the second process, the CIP was suspended in the medium or grease and stirred about 2 h. The sample was varied into five different compositions, by changing the CIP weight percentages. The variations are MR grease with CIPs content of 10% of the total weight or 10 wt% (MG10), 30 wt% (MG30), 50 wt% (MG50), 70 wt% (MG70), and 80 wt% (MG80). The equivalent volume fractions of the CIPs are 0.013, 0.048, 0.105, 0.214, and 0.319, respectively.

4.2. Rheological characterization

The rheological characterization is carried out using parallel-plate rheometer (Anton Paar, MCR 302) equipped with MRD 70 and PP-20 mm measurement tools (rotor with 20 mm plate). The target of the rotational measurement is to obtain the flow curve (shear stress as a function of shear rate) at various magnetic fields. Each data set was obtained by making sure the data has consistency while repeats the same

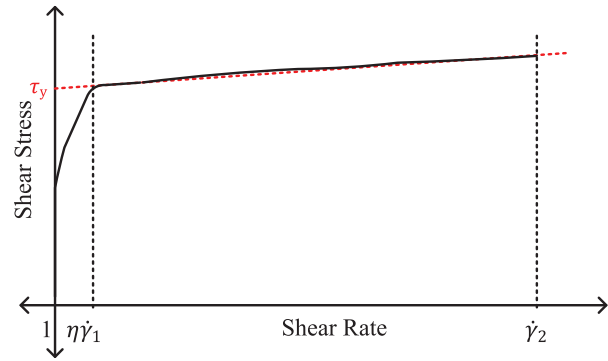


Figure 2. Illustration of the defined yield stress using Bingham plastic model.

configuration and materials three times. The magnetic fields were varied at 0, 0.17, 0.37, 0.50, 0.77, and 0.90 Tesla, while the shear rates data were set between 0 and 2000 s^{-1} with data sampling setting on the logarithmic ramp. However, some of the data cannot reach a shear rate of 2000 s^{-1} because of the limitation of the allowable torque of the rheometer motor. For example, the shear rate for MG80 at 0.77 and 0.90 Tesla can only reach about 200 and 400 s^{-1} , respectively. Therefore, the rheological properties of MG80 are only utilized as training data for the learning material of the proposed model. Meanwhile, for the benchmark of the yield stress prediction, the utilized data sets are for all samples except for MG80.

4.3. Data sets

The total number of the samples, N , is 900 points consisting of 30 different data sets. Each data set represents a flow curve with different weight percentages of CIP and magnetic fields. The data sets were divided into two parts, which are “modeling” and “testing” data sets that can be observed further in Table 1. In order to build the model, two parts of the modeling data sets consisting of train and validation were predefined. The training data were selected randomly with 80% of the modeling data population are used to train the shear stress model; therefore, the data sets can be denoted as Tr. The validation data are 20% of the modeling data to check the model performance with the value of the input near to the training data ranges. This testing data were also denoted as Ts1. Meanwhile, the other type of testing data sets or “unlearned” data were utilized to evaluate the generalization capability of the model to predict the data with the input values far or outside of the training data ranges. The unlearned data were divided into three cases, which are the fixed magnetic field value (Ts2), the fixed solid weight percentage of CIPs value (Ts3), and the combination of Ts2 and Ts3, namely Ts4. The function of Ts3 is to check the generalization capability of the model to predict the effect of

Table 1. The data sets for training and validation.

Data sets	Population	Weight percentage (wt%)	Magnetic fields (Tesla)	Remark
Training data 1 (Tr)	480	10, 30, 50, 80	0, 0.17, 0.37, 0.77, 0.9	Training data sets consisting of 80% of the modeling data
Testing data 1 (Ts1)	120	10, 30, 50, 80	0, 0.17, 0.37, 0.77, 0.9	Validation data sets consisting of 20% of the modeling data
Testing data 2 (Ts2)	150	10, 30, 50, 70, 80	0.50	Unlearned data for fixed magnetic field
Testing data 3 (Ts3)	180	70	0, 0.17, 0.37, 0.5, 0.77, 0.9	Unlearned data for fixed weight percentage
Testing data 4 (Ts4)	300	10, 30, 50, 70, 80	0, 0.17, 0.37, 0.5, 0.77, 0.9	Combination of testing cases of Ts2 and Ts3

Table 2. The accuracy of the proposed model at various data sets for ANN and ELM models.

Data	ANN 15		ANN 25		ELM-HL		ELM-Sin		ELM-Sig	
	RMSE (kPa)	R^2	RMSE (kPa)	R^2	RMSE (kPa)	R^2	RMSE (kPa)	R^2	RMSE (kPa)	R^2
Tr	0.560	0.999	0.475	0.999	0.001	1.000	1.613	0.994	2.079	0.989
Ts1	0.623	0.999	0.721	0.999	0.700	0.999	1.804	0.993	2.275	0.988
Ts2	6.056	0.861	3.627	0.950	3.715	0.948	3.473	0.952	3.926	0.943
Ts3	8.037	0.836	7.294	0.865	3.797	0.968	5.081	0.906	5.812	0.876
Ts4	7.204	0.852	5.916	0.900	3.760	0.962	4.423	0.928	5.043	0.909

ANN: artificial neural network; ELM: extreme learning machine; RMSE: root mean square error; HL: hard limit.

various unknown compositions at a fixed magnetic field value. While Ts2 focuses on the evaluation of various unknown magnetic fields effect at a fixed composition value, Ts4 can be considered as the summary of the unlearned data including Ts2 and Ts3.

4.4. ELM parameters for simulation

The complete set up of the shear stress model, BP-ANN, and ELM algorithm are discussed in this section. The hidden node numbers of ANN were varied from 10 to 50 with sigmoid activation function. The simulations were carried out 20 times and the averages accuracy was recorded and compared with the accuracy of the ELM. Meanwhile, the hidden node number of ELM (L) was varied from 10 to 50,000. The applied activation functions for ELM are hard limit, sinusoid, and sigmoid as defined in equations (12) to (14), respectively. The continuous distribution to assign the weight inputs and biases of SLFN of the ELM models is Gaussian distribution continuous function. The input data for ELM and ANN were normalized using a logarithmic scale for shear rate and linear scale for the other inputs. Then, the input weight and bias were determined using a continuous function, Gaussian distribution.

The model performance is measured based on root mean square error (RMSE) and the coefficient of determinant or correlation factor (R^2), which are expressed in equations (16) and (17), respectively, where τ_e , τ_p , and τ_{mean} are the measured, predicted, and mean of the

shear stress data, respectively. Meanwhile, N is the data number in a data set

$$RMSE = \sqrt{\frac{\sum_i^N (\tau_e - \tau_p)^2}{N}} \quad (16)$$

$$R^2 = 1 - \frac{\sum_i^N (\tau_p - \tau_e)^2}{\sum_i^N (\tau_e - \tau_{e,mean})^2} \quad (17)$$

5. Results and discussion

5.1. Predicted shear stress evaluation

The performance of the proposed model is then evaluated by comparing the shear stress values of the model with the actual measured data and rheological characteristics through the use of both the training and unlearned data of two various data sets, namely, the magnetic fields and CIP weight percentages. The accuracy levels of the various techniques that were used in the training and testing data sets are shown in Table 2. As seen from the table, the BP-ANN models that were configured at 15 (BP-ANN 15) and 25 (BP-ANN 25) hidden node numbers had exhibited a high training but low testing accuracy levels, particularly at the unlearned weight percentage (Ts3), hence denoting the possibility of a model overfitting issue (Zhang and Friedrich, 2003). As for the ELM, this model was found to have produced the least error in both the training and testing stage of its activation function of hard limit (ELM-HL), specifically for all the unlearned magnetic field

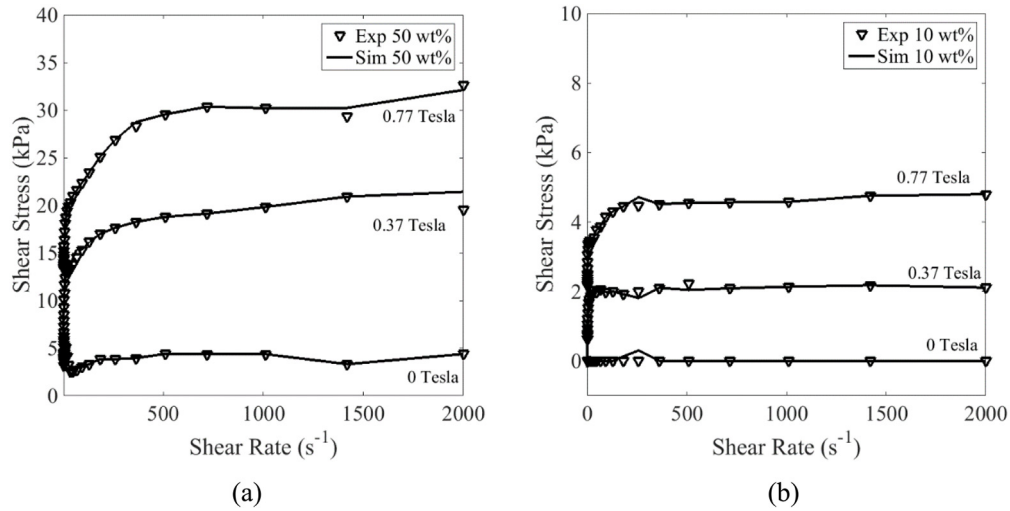


Figure 3. The comparison between the experimental and ELM HL simulation results of the training data (Tr) for various magnetic fields at (a) MG50 and (b) MG10.

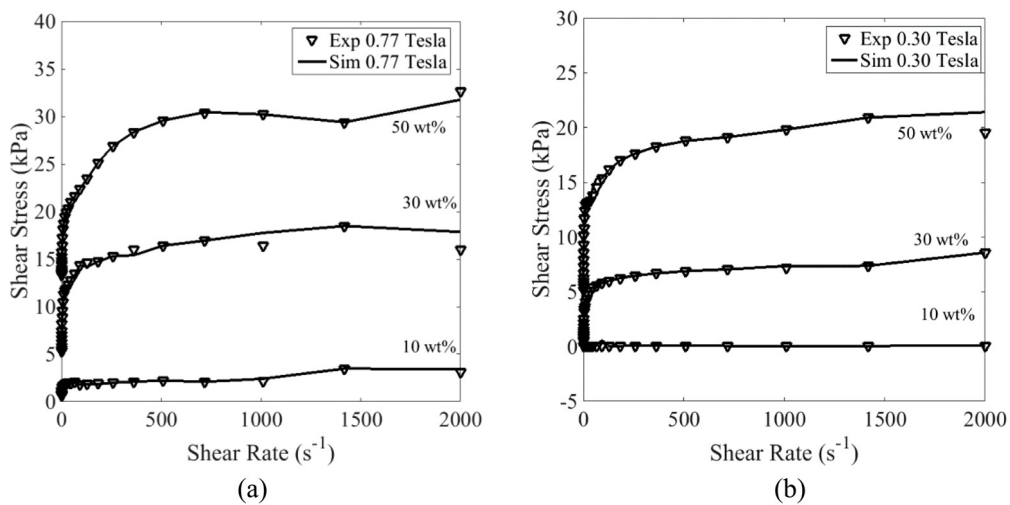


Figure 4. The comparison between the experimental and ELM HL simulation results of the training data (Tr) for various weight percentage of CIPs at (a) 0.77 Tesla and (b) 0.30 Tesla.

(Ts3) and unlearned data (Ts3). During the testing stage for the unlearned magnetic field (Ts2), the ELM with a sine activation function (ELM-Sin) was found to have provided the best accuracy level since the rest of the models had exhibited R^2 values exceeding that of 0.900. In general, the ELM models had not only provided a relatively better accuracy level for the testing data than the ANN 15 and ANN 25, but it was also proven to have a better generalization capability than the ANN models (Huang et al., 2012). For these reasons, the ELM was selected as part of the proposed platform's performance analysis.

The graphical evaluations of the model performance for the various magnetic fields and different CIP weight percentages of the training data sets are shown in

Figures 3 and 4, respectively. On the whole, it can be concluded that the model had matched the shear stress characteristic, particularly at the post-yield or high shear rate regions. The model had not only identified the pattern of the rheological properties at various magnetic fields and CIP weight percentages through the comparison of the measured data and the simulated outputs, the shear stress data of the simulation outputs and experimental results had also exhibited the same visual pattern at the pre-yield or low shear rate regions. Before looking into the detail of the model's capability for replicating the rheological behavior of different materials, it would be best to analyze how the proposed model had fared in its ability for reproducing the fundamental behavior of MR grease at different magnetic

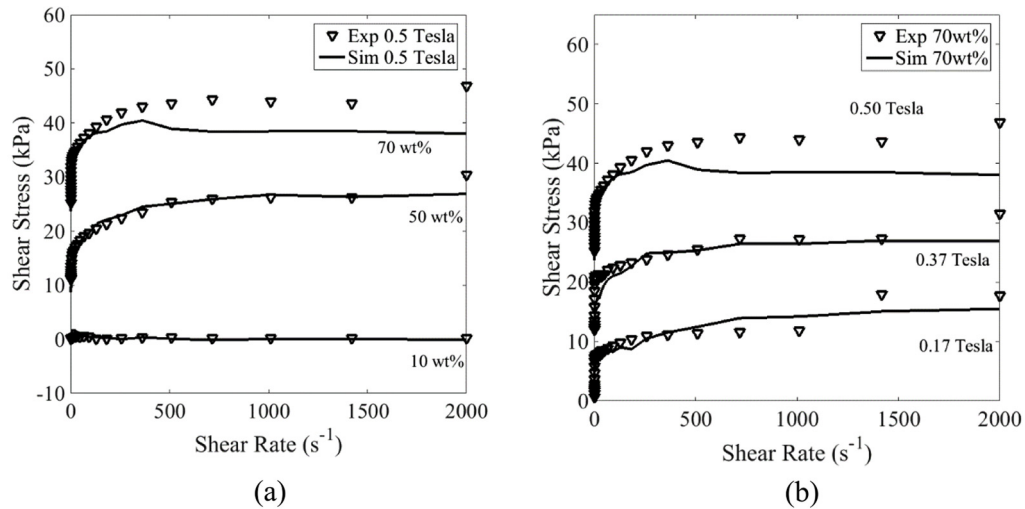


Figure 5. The comparison between the experimental and ELM HL simulation results of the unlearned data at (a) 0.5 Tesla (Ts2) and at (b) 70 wt% (Ts3).

field levels. As shown in Figure 3, the presence of a higher magnetic field had led to a higher shear stress caused by the stronger interaction among the aligned magnetic particles. The effects of the different compositions on the material performances were also successfully replicated as those shown in Figure 4. Since an increased MR effect from the higher shear stress had been observed from those with higher CIP weight percentages, this implies that the single model had been able to replicate the behaviors of field-dependent MR grease at different compositions and magnetic field levels. It is interesting to note that the MR grease, unlike that of the MR fluid, has an initial yield stress at the off-state condition, where the addition of CIPs was found to have improved both the yield stress ($\tau_{y,B}$) and off-state yield stress ($\tau_{y,0}$) simultaneously, with the latter resulting in a smaller value of $E_{\tau_{y,B}}$. From the design application point of view, the ideal value of the initial yield stress should be as small as possible so as to accommodate for the wider operating range of the device.

The acceptance of the ANN model would generally depend on its performance in the shear stress prediction of the unlearned data. According to the ELM theory, the model is deemed to have a generalization capability if the accuracy level of the unlearned data is located out of the training data range. As such, the MR grease model had fulfilled the above criteria by successfully identifying the rheological behavior of the MR grease as a function of shear rate, the unlearned magnetic field, and the CIP weight percentages. Also, the visual observations of the shear stress prediction at the unlearned data could be observed in Figure 5(a) and (b) for the unlearned magnetic fields and the unlearned composition at MG70, respectively. In Figure 5, both the predicted shear stress and experimental data at

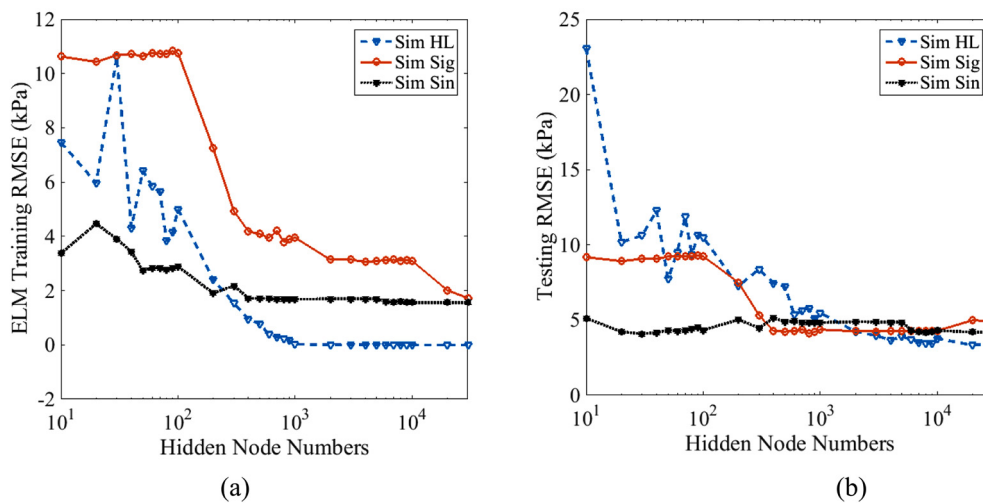
various weight percentages for the unlearned magnetic field intensities were found to have shared the same pattern or behavior. For the unlearned data set of the MG70, although the RMSE for the predicted shear stress had been the highest among all of the different data sets shown in Table 2, the model had, however, shown its ability for predicting the same pattern or behavior of the unknown material, particularly at the post-yield region. Even so, errors that could be visually observed in Figure 5(a) were found to have occurred in the MG70 data set at 0.5 Tesla during the prediction of a data set with unlearned magnetic fields and weight percentages. Therefore, these results suggest that if the user had needed to predict the performance of an unknown composition, then the comparison should be carried out in a learned rather than the unlearned magnetic field. For example, the results in Figure 5(b) had shown the shear stress prediction of MG70 in the learned magnetic field (0.17 and 0.37 Tesla) to have a better accuracy level than that of the unlearned magnetic field (0.5 Tesla).

Since the performances of the proposed models in the training and testing data are mainly affected by the normalization method and the hidden node numbers, the detailed information of these two parameters is therefore discussed in the subsequent paragraphs. To begin with, the normalization methods from equations (7) to (9) were selected because they had been proven to be far superior to the rest of the methods. In Table 3, the possible normalization methods of the inputs (shear rate ($\dot{\gamma}$), magnetic field (B), and solid weight percentage (w_i)) were compared in terms of the predicted shear stress accuracy/RMSE using the ELM HL. From the comparison results, the configuration nos 4 (equations (7) to (9)) and 5 were then selected based on their testing accuracy levels and generalization capabilities that

Table 3. The accuracy of the ELM HL using some normalization possibilities.

No.	Input parameters			Training		Test		Δ RMSE
	$\dot{\gamma}$	B	w_t	RMSE (Pa)	R^2	RMSE (Pa)	R^2	
1	lin	lin	lin	347	1.000	5815	0.901	6162
2	lin	lin	log	331	1.000	6475	0.863	6805
3	lin	log	lin	309	1.000	5327	0.915	5636
4	log	lin	lin	1	1.000	3730	0.960	3729
5	log	log	lin	1	1.000	3720	0.960	3719
6	log	lin	log	1	1.000	4625	0.929	4624
7	lin	log	log	300	1.000	19,399	—	19,699
8	log	log	log	1	1.000	4603	0.931	4602

ELM: extreme learning machine; HL: hard limit; RMSE: root mean square error.

**Figure 6.** The effect of the hidden node numbers of the ELM models for (a) training and (b) testing case of Ts4.

relatively better than other methods. Configuration nos 4 and 5 have similarity in terms of the normalization method of $\dot{\gamma}$ and w_t using logarithm and linear normalization, respectively. The same patterns were also observed in the ELM Sin and Sig. For $\dot{\gamma}$, it could be resulted from the similarities of the shear rate and stress correlation of the shear thinning behavior it shared with the logarithm pattern. While using linear normalization for $\dot{\gamma}$ of 1, 2, 3, and 7, the testing of the RMSEs increases up to 2 kPa. Moreover, for normalized w_t , the linear normalization method has produced better results than using log, while other inputs have the same normalization method, such as nos 1 and 2.

The parametric studies for the hidden node number were then carried out for the ELM and ANN. For ELM, the hidden node number of 10,000 was carried out because the accuracy levels of the ELM HL, Sig, and Sin had shown relatively consistent values as shown in Figure 6. While it is still possible to select the other hidden node numbers between 2000 and 10,000 with a reasonable training time (about 1–4 s) and the testing

data of below 5 kPa for the RMSE, it is important to note that the addition of hidden node numbers exceeding 10,000 would still produce the same results (except ELM Sig) but with a higher computational burden. As seen from Figure 7, the average of the BP-ANN's training error after 50 runs was found to have declined with the increasing hidden node numbers, while no pattern was observed from the hidden node effect of the Ts4 testing case. Although the RMSE was found to have increased from 25 to 40 hidden node numbers, it had nevertheless demonstrated a drop at hidden node numbers of 15, 25, and 50. The boxplot results of RMSE testing case in Figure 8 had also shown the BP-ANN having a relatively wider range of more than 25 kPa at hidden node numbers of 10, 20, 35, and 40 as compared to the ELM models that have relatively lower variants or standard deviations at repeated trainings. The wider range of the BP-ANN could be explained by its possibility of being trapped at a local minimum value during the running of the iterations. Furthermore, the BP-ANN training time has wide range possible durations

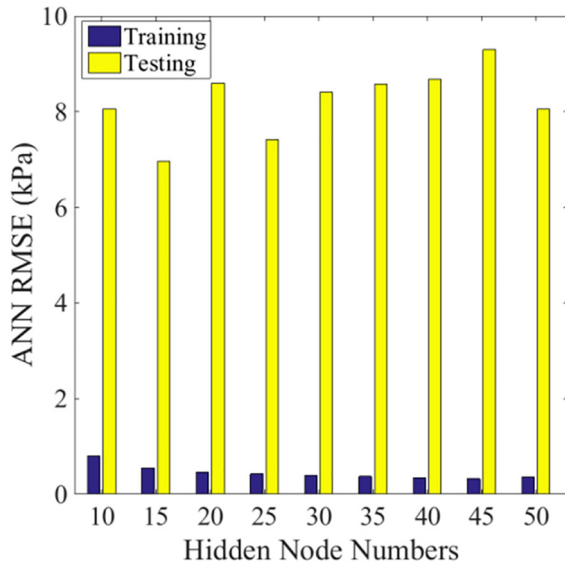


Figure 7. The effect of the hidden node numbers to BP-ANN performance for training and testing case of Ts4.

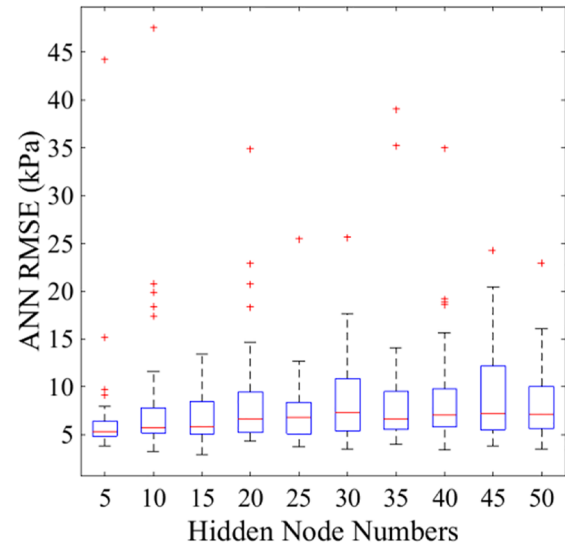


Figure 8. Boxplot of the testing RMSE (Ts4) of BP-ANN at various hidden node numbers.

Table 4. The accuracy of the predicted apparent viscosity at various data sets for ANN and ELM.

Data	ELM HL		ELM Sin		ELM Sig		ANN 25	
	RMSE (Pa s)	R ²	RMSE (Pa s)	R ²	RMSE (Pa s)	R ²	RMSE (Pa s)	R ²
Tr	0	1.000	5316	0.992	8138	0.982	1437	0.999
Ts1	513	1.000	2284	0.996	3016	0.993	4158	0.997
Ts2	8105	0.975	6567	0.983	7040	0.981	6619	0.983
Ts3	3881	0.997	13737	0.957	15485	0.945	13193	0.960
Ts4	6171	0.989	11070	0.966	12382	0.957	10717	0.968

ANN: artificial neural network; ELM: extreme learning machine; RMSE: root mean square error.

depending on the required iteration to reach the pre-determined termination conditions ranging from 2 to 15 s.

5.2. Predicted viscosity and yield stress evaluation

The proposed model had consisted of two derived outputs, namely, the apparent viscosity and yield stress for determining the MR grease performance. As shown in Table 4, the predicted apparent viscosity from the ELM and ANN models under the training data was found to be in good agreement with the expected experiment outcome. Moreover, the apparent viscosity prediction of the unlearned data as depicted in Figure 9 had demonstrated fewer errors than those of the ANN method, particularly at the unlearned or unknown magnetic field (Ts2) and composition (Ts3) levels. Meanwhile, the experimental yield stress of the validation data was also compared with a predicted yield stress and was found to have corresponded to the same pattern as shown in Figure 10. While “the experimental yield stress” is

obtained from the shear stress experimental data of between 300 and 2000 s⁻¹ that was fitted into the Bingham plastic model (see section 3.2), the predicted yield stress is calculated based on the predicted shear stress by the proposed machine learning models. The accuracy of R² for all the ELM HL, ELM Sin, and ELM Sig gathered data (except MG80), as depicted in Table 5, had shown the respective ELM Sin and Sig achieving the best and least prediction with R² of 0.982 and 0.977. At MG70 (ELM grease with CIPs content of 70 wt%), the predicted yield stress was found to be the main contributor of the errors, particularly at a high magnetic field with a yield stress of below 60 kPa at 0.77 Tesla as opposed to the 64 kPa set in the experimental yield stress. Although further improvement is still required in the model prediction of the yield stress for MG70, its prediction on the other compositions had, however, yielded an agreeable pattern. It is also interesting to note that the yield stress values of MG10 during the off-state condition at ELM Sin and Sig had depicted negative values, which could be due to the

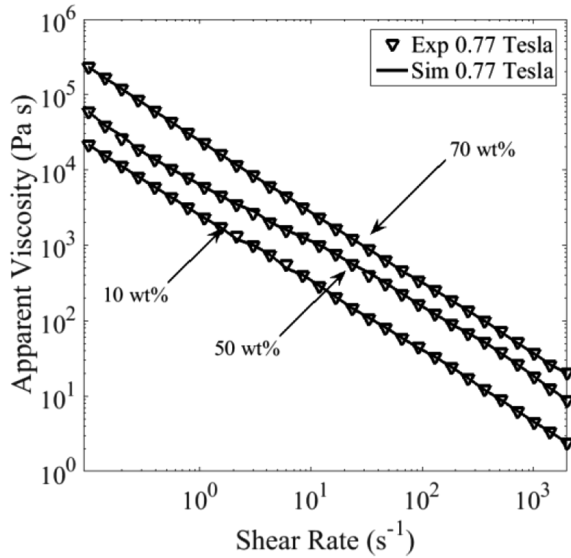


Figure 9. The visual comparison of the predicted apparent viscosity using ELM HL at a magnetic field of 0.77 Tesla.

ELM algorithm trying to obtain the best accuracy level or the least errors with respect to the predicted shear stress. As a result, the yield stress of the MG10 at an off-state condition with a shear stress range of between 0 and 3 kPa was found to have produced a higher error than the others. Although the ELM Sin was revealed to have produced the best accuracy level, its settings, however, are not recommended for those with lower weight percentage applications (MG10) since it would be impossible for the negative values at off-state yield stress ($\tau_{y,0}$) that was produced in the prediction to occur in the characterization process. For this reason, the predicted yield stress that was based on the ELM Hardlim was chosen for not only exhibiting a yield stress with an R^2 accuracy of 0.979 but also producing non-negative values from its prediction results. Hence, apart from its ability of predicting the yield stress at various magnetic fields, the models had similarly proven their capabilities for predicting the thixotropic properties of the MR grease as shown by the yield stress existence at zero magnetic fields or in an off-state condition.

The predicted yield stress of the proposed ELM models had also been compared with the existing model (simulated from equation (2)) suggested by Varela-Jiménez et al. (2015) as shown in Table 5, where the values of the respective B_{MRF} , $\xi(3)$, K , M_s , μ_0 , α , β_v , and λ had been 2.41, 1.202, 6, 831.23 kA m⁻¹, $4\pi \times 10^{-7}$ H m⁻¹, -1547.2 kA m⁻¹, 2532 kA m⁻¹, and -30.544 kA m⁻¹. The proposed ELM model had therefore shown its superiority in terms of its accuracy levels and pattern recognition capabilities since the visual observations of the constitutive model in Figure 10 had shown inconsistent patterns of the predicted yield stress when the magnetic fields were changed from the low to the high magnetic regions as a

Table 5. The accuracy of the yield stress in various cases on different data sets.

Scheme	RMSE (kPa)	R^2
ELM HL	3.281	0.979
ELM Sig	3.423	0.977
ELM Sin	3.013	0.982
ANN 25	3.493	0.977
STE	7.481	0.815

STE: state transition equation; ANN: artificial neural network; ELM: extreme learning machine; RMSE: root mean square error.

result of the broader range of the CIP volume fraction (between 0.013 and 0.319) used in this study as opposed to the smaller range (0.22, 0.32, and 0.4) suggested by Varela-Jiménez et al. (2015). Another reason for the inaccuracies could also be described from the calculation process and the complexity of equation (2), where it had consisted of a polynomial model that is known for its unpredictability at a more extensive input variable range. The process to obtain the best fit model also has to consider the possibility of the equation $\alpha\varphi^2 + \beta_v\varphi + \lambda < 0$ with a certain B_{MRF} value producing a complex number. Since the constitutive model was also developed based on the state transition phenomena of the MR fluids, where the MR fluids were assumed to exhibit a Newtonian fluid behavior at zero magnetic field exposure, this had therefore demonstrated the existing model's inability of including the yield stress at the off-state condition, which were shown by the zero yield stress values at various weight percentages during the off-state condition in Figure 11. For that reason, it is suggested that the yield stress variable at the off-state condition is added in the model as a way of further investigating its effect on the material composition.

In summary, the proposed model had shown its capability in not only the simultaneous replication and prediction of both the shear and yield stress with an acceptable error for the learned and unlearned data, but the graph patterns had also been verified to be similar to those of the experimental data from the rotational mode. As such, this model can be taken into consideration during the material designing stage, since it had offered preferably smaller yield stress at the off-state condition or a possible maximum yield stress. However, the model would still require further improvement with regard to the discrepancies found in the lower magnetic field region as well as its scalability for those with different configurations. An improvement to reduce the error can, therefore, be initiated by examining the model configurations such as its normalization, the activation function, as well as the hidden node numbers. It is important to note that the scope of this study had been limited by the model development of a rotational test in the observation of the MR grease performance. The data from the rheological properties are deemed to be

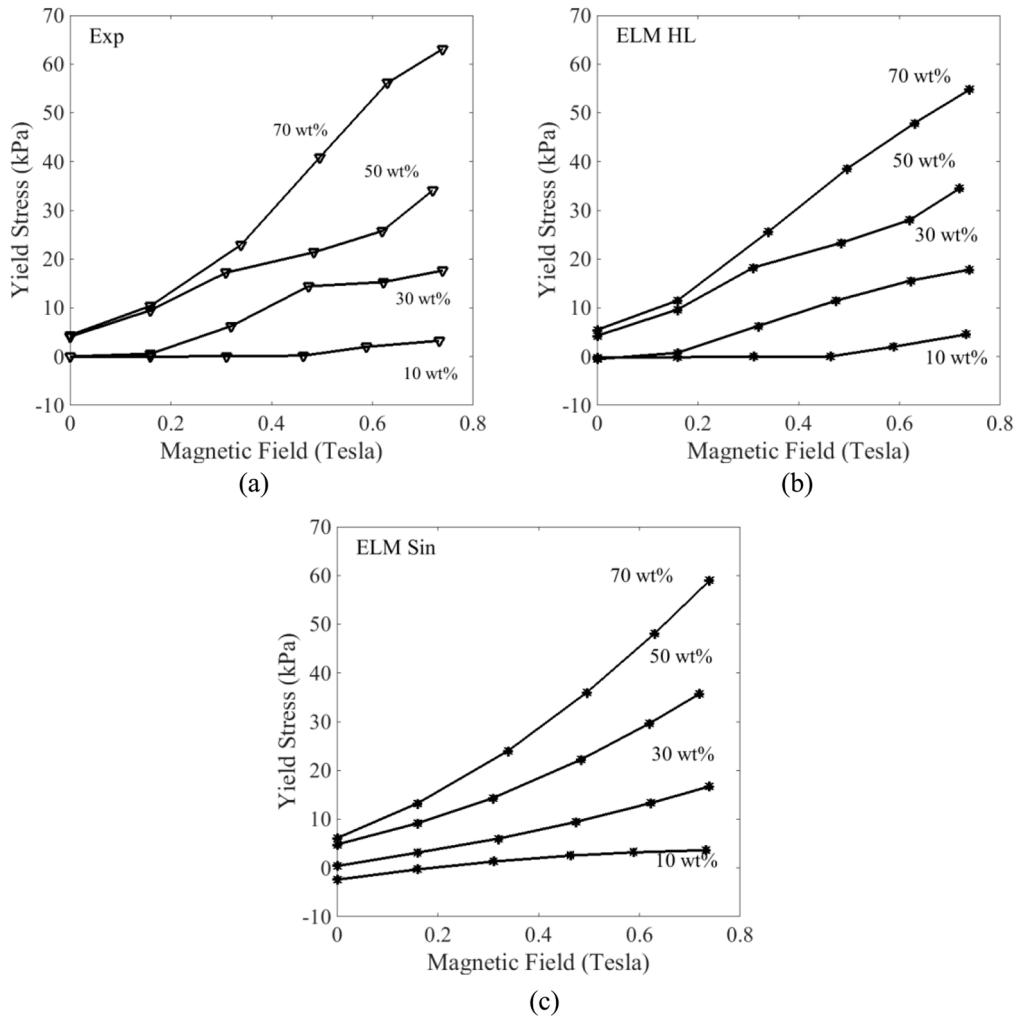


Figure 10. The comparison between (a) the experimental, simulation results of ELM, (b) Hardlim, (c) Sinusoid of the yield stress based on fitting of Bingham plastic model at shear stress between the shear rate of 500 and 2000 s^{-1} .

sufficient for designing certain MR devices such as the MR brake, but may not be applicable for the semi-active vibration control application cases that require more critical viscoelastic properties from the oscillation test. As such, it will be interesting to consider the viscoelastic properties in the construction of a modeling framework for the MR grease. Finally, the model should also consider incorporating at least four inputs of shear strain, frequency, magnetic field, and solid weight percentage and one storage modulus output as a way of achieving a more effective oscillation test.

6. Conclusion

The MR greases were fabricated by varying the CIP weight percentages and characterizations, where the shear rate and magnetic field effects were observed by using a parallel-plate rheometer. As shown from the characterization study, the addition of the CIP volume

fraction was found to have led to a higher shear and yield stress while simultaneously increasing the off-state yield stress. A unified model of the MR grease was also designed to predict the shear stress, apparent viscosity, and yield stress with the shear stress model constructed from a selection of the BP-ANN and ELM machine learning methods. With the composition (the weight percentage of CIPs) being a model input as well as the shear rate and magnetic fields as the operating variables, the model was then evaluated under different cases of various data sets. The generalization capabilities for predicting the rheological behavior at unlearned or unknown composition and magnetic fields were also evaluated and compared with the experimental results. Although the ELM or BP-ANN were found to be the most suitable models chosen, the ELM models had proven its prediction superiority at unlearned data, particularly those with unlearned magnetic field and composition. The ELM also has the

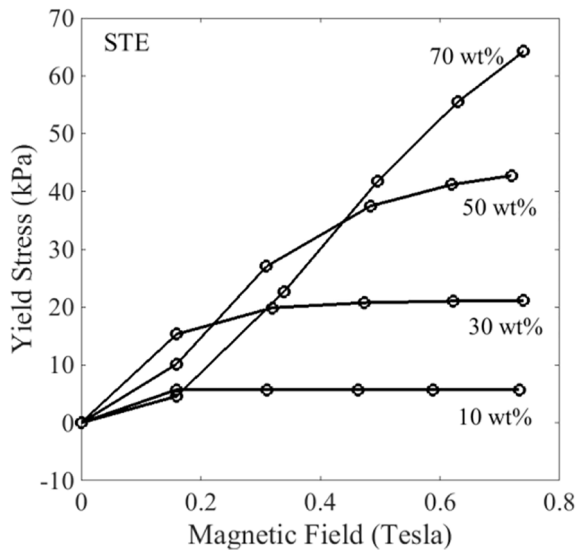


Figure 11. The yield stress prediction based on STE model (equation (2)).

potential for predicting the rheology materials as it had avoided the over-fitting issue and possessed a better-generalizing performance. As for the apparent viscosity and yield stress estimator, they too were developed and evaluated at various weight percentages and magnetic fields, where the prediction was shown to have produced better results than the existing constitutive equations. This proposed model can therefore be utilized in the prediction of the MR grease rheological behavior at multiple compositions during the material development stage or in the design of MR grease devices. The material development of the MR greases can also be further investigated through the incorporation of additives and various compositional shapes into the model. Finally, this model can be further improved by examining its inputs normalization, the ELM activation function, and hidden node numbers.


Declaration of conflicting interests


The author(s) declared no potential conflicts of interest with respect to the research, authorship, and/or publication of this article.

Funding

The author(s) disclosed receipt of the following financial support for the research, authorship, and/or publication of this article: This work was supported by the Universiti Teknologi Malaysia under TDR (Vot No: 07G19) and Universitas Sebelas Maret through International Collaboration Grant 2019 (ID:66502032019).

ORCID iDs

Irfan Bahiuddin  <https://orcid.org/0000-0001-9070-3348>

Norzilawati Mohamad  <https://orcid.org/0000-0002-3113-6598>

References

- Ashtiani M, Hashemabadi SH and Ghaffari A (2015) A review on the magnetorheological fluid preparation and stabilization. *Journal of Magnetism and Magnetic Materials* 374: 716–730.
- Bahiuddin I, Mazlan SA, Shapiai MI, et al. (2017) Study of extreme learning machine activation functions for magnetorheological fluid modelling in medical devices application. In: *International conference on robotics, automation and sciences (ICORAS)*, Melaka, Malaysia, 27–29 November, pp. 1–5. New York: IEEE.
- Bahiuddin I, Mazlan SA, Shapiai MI, et al. (2018a) A new constitutive model of a magneto-rheological fluid actuator using an extreme learning machine method. *Sensors and Actuators A: Physical* 281: 209–221.
- Bahiuddin I, Mazlan SA, Shapiai MI, et al. (2018b) Constitutive models of magnetorheological fluids having temperature-dependent prediction parameter. *Smart Materials and Structures* 27(9): 095001.
- Bahiuddin I, Mazlan SA, Shapiai MI, et al. (2019) A new platform for the prediction of field-dependent yield stress and plastic viscosity of magnetorheological fluids using particle swarm optimization. *Applied Soft Computing* 76: 615–628.
- Bobbili R, Madhu V and Gogia AK (2014) Neural network modeling to evaluate the dynamic flow stress of high strength armor steels under high strain rate compression. *Defence Technology* 10(4): 334–342.
- Bucchi F, Forte P and Frendo F (2015) Analysis of the torque characteristic of a magnetorheological clutch using neural networks. *Journal of Intelligent Material Systems and Structures* 26(6): 680–689.
- Chang C-C and Zhou L (2002) Neural network emulation of inverse dynamics for a magnetorheological damper. *Journal of Structural Engineering* 128(2): 231–239.
- Choi HJ, Zhang WL, Kim S, et al. (2014) Core-shell structured electro- and magneto-responsive materials: fabrication and characteristics. *Materials* 7(11): 7460–7471.
- Choi YT, Cho JU, Choi SB, et al. (2005) Constitutive models of electrorheological and magnetorheological fluids using viscometers. *Smart Materials and Structures* 14(5): 1025–1036.
- Cvek M, Mrlik M and Pavlinek V (2016) A rheological evaluation of steady shear magnetorheological flow behavior using three-parameter viscoplastic models. *Journal of Rheology* 60(4): 687–694.
- De Vicente J, Klingenberg DJ and Hidalgo-Alvarez R (2011) Magnetorheological fluids: a review. *Soft Matter* 7(8): 3701–3710.
- Dimock GA, Lindler JE and Wereley NM (2000) Bingham biplastic analysis of shear thinning and thickening in magnetorheological dampers. *Proceedings of SPIE—The International Society for Optical Engineering* 3985: 444–455.
- Dimock GA, Yoo J-H and Wereley NM (2002) Quasi-steady Bingham biplastic analysis of electrorheological and magnetorheological dampers. *Journal of Intelligent Material Systems and Structures* 13(9): 549–559.

- Farjoud A, Vahdati N and Fah YF (2008) Mathematical model of drum-type MR brakes using Herschel-Bulkley shear model. *Journal of Intelligent Material Systems and Structures* 19(5): 565–572.
- Ghaffari A, Hashemabadi SH and Ashtiani M (2015) A review on the simulation and modeling of magnetorheological fluids. *Journal of Intelligent Material Systems and Structures* 26(8): 881–904.
- Ginder JM, Davis LC and Elie LD (1996) Rheology of magnetorheological fluids: models and measurements. *International Journal of Modern Physics B* 10(23n24): 3293–3303.
- Gurubasavaraju TM, Kumar H and Arun M (2017) Evaluation of optimal parameters of MR fluids for damper application using particle swarm and response surface optimisation. *Journal of the Brazilian Society of Mechanical Sciences and Engineering* 39(9): 3683–3694.
- Huang G, Huang G-B, Song S, et al. (2015) Trends in extreme learning machines: a review. *Neural Networks* 61: 32–48.
- Huang G-B, Wang DH and Lan Y (2011) Extreme learning machines: a survey. *International Journal of Machine Learning and Cybernetics* 2(2): 107–122.
- Huang G-B, Zhou H, Ding X, et al. (2012) Extreme learning machine for regression and multiclass classification. *IEEE Transactions on Systems, Man, and Cybernetics, Part B (Cybernetics)* 42(2): 513–529.
- Imaduddin F, Mazlan SA, Ubaidillah, et al. (2017) Characterization and modeling of a new magnetorheological damper with meandering type valve using neuro-fuzzy. *Journal of King Saud University—Science* 29(4): 468–477.
- Jin W, Liu Y and Gao Z (2017) Fast property prediction in an industrial rubber mixing process with local ELM model. *Journal of Applied Polymer Science* 134(41): 45391.
- Jung ID, Kim M and Park SJ (2016) A comprehensive viscosity model for micro magnetic particle dispersed in silicone oil. *Journal of Magnetism and Magnetic Materials* 404: 40–44.
- Karakoc K, Park EJ and Suleman A (2008) Design considerations for an automotive magnetorheological brake. *Mechatronics* 18(8): 434–447.
- Khozani ZS, Bonakdari H and Zaji AH (2017) Efficient shear stress distribution detection in circular channels using Extreme Learning Machines and the M5 model tree algorithm. *Urban Water Journal* 14: 999–1006.
- Kim JE, Ko J-D, Liu YD, et al. (2012) Effect of medium oil on magnetorheology of soft carbonyl iron particles. *IEEE Transactions on Magnetics* 48(11): 3442–3445.
- Leong SAN, Mohd Samin P, Idris A, et al. (2016) Synthesis, characterization and magnetorheological properties of carbonyl iron suspension with superparamagnetic nanoparticles as an additive. *Smart Materials and Structures* 25(2): 25025.
- Li W, Wei S, Jiao W, et al. (2016) Modelling of adsorption in rotating packed bed using artificial neural networks (ANN). *Chemical Engineering Research and Design, Institution of Chemical Engineers* 114: 89–95.
- Liu Y and Chen J (2013) Integrated soft sensor using just-in-time support vector regression and probabilistic analysis for quality prediction of multi-grade processes. *Journal of Process Control* 23(6): 793–804.
- Liu Y, Fan Y and Chen J (2017) Flame images for oxygen content prediction of combustion systems using DBN. *Energy & Fuels* 31(8): 8776–8783.
- Liu Y, Li C and Gao Z (2014) A novel unified correlation model using ensemble support vector regression for prediction of flooding velocity in randomly packed towers. *Journal of Industrial and Engineering Chemistry* 20(3): 1109–1118.
- Liu Y, Yang C, Gao Z, et al. (2018) Ensemble deep kernel learning with application to quality prediction in industrial polymerization processes. *Chemometrics and Intelligent Laboratory Systems* 174: 15–21.
- Marinică O, Susan-Resiga D, Bălănean F, et al. (2016) Nano-micro composite magnetic fluids: magnetic and magnetorheological evaluation for rotating seal and vibration damper applications. *Journal of Magnetism and Magnetic Materials* 406: 134–143.
- Mohamad N, Mazlan SA, Ubaidillah, et al. (2016) The field-dependent rheological properties of magnetorheological grease based on carbonyl-iron-particles. *Smart Materials and Structures* 25(9): 095043.
- Mohamad N, Ubaidillah, Mazlan SA, et al. (2018) A comparative work on the magnetic field-dependent properties of plate-like and spherical iron particle-based magnetorheological grease. *PLoS ONE* 13(4): e0191795.
- Mueller T, Kusne AG and Ramprasad R (2016) Machine learning in materials science. *Reviews in Computational Chemistry* 29(1): 186–273.
- Papanastasiou TC (1987) Flows of materials with yield. *Journal of Rheology* 31(5): 385–404.
- Papanastasiou TC and Boudouvis AG (1997) Flows of viscoplastic materials: models and computations. *Computers & Structures* 64(1–4): 677–694.
- Rabbani Y, Shirvani M, Hashemabadi SH, et al. (2017) Application of artificial neural networks and support vector regression modeling in prediction of magnetorheological fluid rheometry. *Colloids and Surfaces A: Physicochemical and Engineering Aspects* 520: 268–278.
- Sahin H, Wang X and Gordaninejad F (2009) A new model for yield stress of magneto-rheological greases/gels under combined effects of magnetic field and temperature. *Proceedings of SPIE—The International Society for Optical Engineering* 7288: 72881E.
- Shahriar A and Nehdi ML (2011) Modeling rheological properties of oil well cement slurries using artificial neural networks. *Journal of Materials in Civil Engineering* 23(12): 1703–1710.
- Sherman SG, Becnel AC and Wereley NM (2015) Relating Mason number to Bingham number in magnetorheological fluids. *Journal of Magnetism and Magnetic Materials* 380: 98–104.
- Shilan ST, Mazlan SA, Ido Y, et al. (2016) A comparison of field-dependent rheological properties between spherical and plate-like carbonyl iron particles-based magneto-rheological fluids. *Smart Materials and Structures* 25(9): 095025.
- Tang J, Deng C and Huang G-B (2016) Extreme learning machine for multilayer perceptron. *IEEE Transactions on Neural Networks and Learning Systems* 27(4): 809–821.
- Tang J, Deng C, Huang G-B, et al. (2015) Compressed-domain ship detection on spaceborne optical image using deep neural network and extreme learning machine. *IEEE Transaction on Geoscience and Remote Sensing* 53(3): 1174–1185.

- Vani S, Sukumaran RK and Savithri S (2015) Prediction of sugar yields during hydrolysis of lignocellulosic biomass using artificial neural network modeling. *Bioresource Technology* 188: 128–135.
- Varela-Jiménez MI, Vargas Luna JL, Cortés-Ramírez J, et al. (2015) Constitutive model for shear yield stress of magnetorheological fluid based on the concept of state transition. *Smart Materials and Structures* 24(4): 045039.
- Wang DH and Liao WH (2005) Modeling and control of magnetorheological fluid dampers using neural networks. *Smart Materials and Structures* 14(1): 111–126.
- Wei J, He GT, Song L, et al. (2012) Study of nonspherical particle magnetorheological greases with computer simulation technology. *Applied Mechanics and Materials* 246–247: 1231–1236.
- Xu F-H, Xu Z-D, Zhang X-C, et al. (2015) A compact experimentally validated model of magnetorheological fluids. *Journal of Vibration and Acoustics* 138(1): 011017.
- Xu J, Wang P, Pang H, et al. (2018) The dynamic mechanical properties of magnetorheological elastomers under high strain rate. *Composites Science and Technology* 159: 50–58.
- Yunus NA, Mazlan SA, Ubaidillah, et al. (2016) Rheological properties of isotropic magnetorheological elastomers featuring an epoxidized natural rubber. *Smart Materials and Structures* 25(10): 107001.
- Zhang Z and Friedrich K (2003) Artificial neural networks applied to polymer composites: a review. *Composites Science and Technology* 63(14): 2029–2044.
- Zheng W, Gao X, Liu Y, et al. (2017) Industrial Mooney viscosity prediction using fast semi-supervised empirical model. *Chemometrics and Intelligent Laboratory Systems* 171: 86–92.
- Zheng W, Liu Y, Gao Z, et al. (2018) Just-in-time semi-supervised soft sensor for quality prediction in industrial rubber mixers. *Chemometrics and Intelligent Laboratory Systems* 180: 36–41.